CMS Physics Analysis Summary

Contact: cms-pag-conveners-top@cern.ch 2016/09/23

Bounding the top quark width using final states with two charged leptons and two jets at $\sqrt{s} = 13$ TeV

The CMS Collaboration

Abstract

A direct bound on the top quark decay width is presented, obtained by analysing 12.9 fb^{-1} of proton-proton collision data collected at $\sqrt{s} = 13$ TeV by the CMS experiment at the LHC. The measurement is performed by partially reconstructing the kinematics of top quark candidates from final states containing at least two charged leptons (electrons or muons) and at least two jets, where at least one jet is identified as stemming from the fragmentation and hadronization of a b quark. The observable is compared to the simulated expectations for different top quark width scenarios using a likelihood technique. Under the hypothesis of a standard model-like top quark the measurement yields limits at the 95% CL of $0.6 \leq \Gamma_t \leq 2.5$ GeV, with an expected limit at $0.6 \leq \Gamma_t \leq 2.4$ GeV for a top quark mass of 172.5 GeV.

1 Introduction

In the standard model (SM), the top quark is a fundamental particle with large couplings to the Higgs boson, owing to its mass. Given that the CKM matrix element $V_{tb} \approx 1$, the top quark decays preferentially in Wb final states, before it hadronizes. Although the mass of the top quark is precisely determined to a 0.3% total uncertainty [1] using fully reconstructed top quark decay kinematics compared to simulated predictions, its width, denoted Γ_t, is determined less accurately. Γ_t is a fundamental property of the particle related to the second moment of the top quark mass distribution, and its value is inversely related to the lifetime of the quark.

Several methods have been employed to measure the width of the top quark. Indirect determinations involve a combination of a measurement of the branching fraction $R_b = \frac{\mathcal{B}(t\to Wb)}{\mathcal{B}(t\to Wq)}$ and of the single top t-channel cross section [2]. Using this method D0 has determined $\Gamma_t = 2.00^{+0.47}_{-0.43}$ GeV [3], while CMS has reported $\Gamma_t = 1.36 \pm 0.02(\text{stat.})^{+0.14}_{-0.11}(\text{syst.})$ GeV [4]. Indirect measurements are limited by the knowledge of the b-tagging efficiency (the limiting factor for the extraction of R_b) and the uncertainty in the measurement of the t-channel cross section. Direct determinations of the width have been carried out by the CDF collaboration by reconstructing the top quark mass lineshape and comparing it to simulated predictions. An upper limit of $\Gamma_t < 6.38$ GeV has been obtained at the 95% CL [5], limited by the statistical and jet energy resolution uncertainties. Both direct and indirect determinations are found to agree with the next-to-leading order (NLO) SM prediction $\Gamma_t^{NLO} = 1.35$ GeV, for $m_t = 173.3$ GeV and $\alpha_S = 0.118$ [4], but are still far away from challenging its $< 1\%$ uncertainty.

In this document we present a direct measurement of the top quark width from observables which partially reconstruct the top quark kinematics. By profiting from the higher integrated luminosity datasets of Run 2 of the LHC, which allow for a fine-grained analysis of the observables in different categories, we expect a reduction in the impact of experimental uncertainties affecting the measurement. The current Monte-Carlo (MC) simulations used in CMS are accurate to NLO in production but only to leading order (LO) in the decay of the top quark. As such, the lineshape of the mass distribution is expected to follow that of a relativistic Breit-Wigner distribution. A direct measurement of the width in this regime is expected to be sensitive to missing orders in the MC, as well as to potential beyond-SM sources.

The note is organized as follows: Section 2 describes the data, simulations and event selection employed, Section 3 defines the observable and Section 4 discusses the main uncertainties affecting the measurement. The statistical analysis of the observable is presented in Section 5 and a summary of the results is given in Section 6.

2 Data, simulation and event selection

This measurement is performed using $12.9 \pm 0.8\,\text{fb}^{-1}$ [6] of proton-proton collision data collected at $\sqrt{s} = 13$ TeV by the CMS detector at the CERN LHC. Details on the CMS detector can be found in [7].

All processes involving the double resonant ($t\bar{t}$) and single resonant (tW) productions of top quarks are considered signal in our analysis. The final state decay signature involves at least two charged leptons, two neutrinos and at least one b-jet in the final state. The relative contribution of the two production modes is determined by using the next-to-next-to-leading order (NNLO) [8] and approximate NNLO [9] predictions for the $t\bar{t}$ and tW processes. The $t\bar{t}$ production is modeled with POWHEG v2 [10, 11], while tW is modeled with POWHEG v1 [12]. Both are paired with PYTHIA v8.205 [13, 14]. The NNPDF3.0 NLO [15] parton distribution functions

(PDF) and the CUETP8M1 [16, 17] underlying event tune have been used in the simulation.

The main backgrounds expected in this analysis are due to Drell-Yan (DY), di-boson (WW,WZ, ZZ), W+jets, and single-top (t-channel) production. The latter is not considered as a signal process given that the expected contamination is small and the second reconstructed charged lepton is expected to be from non-prompt sources, e.g. misreconstruction of a signal event from a semi-leptonic b-hadron decay does not affect our result. The MC samples used to model the backgrounds are similar to the ones used in [18].

All simulations include an emulation of the response of the CMS detector using GEANT4 v.9.4p03 [19]. The effects induced by multiple pp collisions are considered for the same and neighbouring beam crossings (within 25 ns) and added to the generated hard interaction, according to the pileup multiplicity which is observed in data.

The data were collected requiring double lepton triggers. We request that at least one of the reconstructed leptons has $p_{\mathrm{T}} > 30$ GeV and $|\eta| < 2.1$, and fullfills tight identification and isolation criteria. These are tighter criteria than the ones used at trigger level. A second lepton with $p_{\mathrm{T}} > 20\,\mathrm{GeV}$ and $|\eta| < 2.5$ is additionally required, fullfilling the same identification and isolation criteria. Events with more than two leptons also pass the selection, provided they satisfy these conditions. The dilepton candidate is expected to have no charge (built from opposite signed charged leptons) and to have an invariant mass $M_{\ell\ell} > 20\,\mathrm{GeV}$. For ee and $\mu\mu$ events the Z pole mass region is used as a control region and excluded from the main analysis by requiring $|M_{\ell\ell} - 91| > 15\,\mathrm{GeV}$. The events are further required to have two jets with $p_{\mathrm{T}} > 30\,\mathrm{GeV}$ and $|\eta| < 4.5$. One of the selected jets is required to be identified as stemming from the fragmentation and hadronization of a b quark by using the medium working point of the Combined Secondary Vertex algorithm (CSVv2) [20]. In our analysis, the events are categorized according to the number of b-tagged jets (=1 or $\geq$2) and the flavour of the dilepton candidate (ee, eμ or $\mu\mu$).

All backgrounds are estimated from simulation, with the exception of the DY contribution. The $R_{in/out}$ method is employed, using the Z pole mass control region in ee and $\mu\mu$ events to determine an overall scale factor which is applied to rescale the DY contribution [18]. In the $e\mu$ channel the scale factor applied is $SF_{\mathrm{DY}}(\mathrm{e}\mu) = \sqrt{SF_{\mathrm{DY}}(\mathrm{ee})SF_{\mathrm{DY}}(\mu\mu)}$. The scale-factors are independently determined for the =1 or $\geq$2 b-tagged jet categories to be in the range of 0.85-0.99. A 30% uncertainty is assigned to these scale factors, in addition to the statistical uncertainty of their determination.

After selection, 66408 (31151) events with =1b- ($\geq$2b-) tagged jets are obtained, with an expected purity of $\approx$ 91% (97%). The total number of expected events agrees with the observations in each individual category used in the analysis.

Figure 1 shows two distributions of the transverse momentum of the systems of leptons and b-tagged jets found in an event ($p_{\mathrm{T}}(\ell,\mathrm{b})$), obtained after pre-selection. The momenta are calculated using an inclusive strategy: up to four pairings are considered per event, whereby up to two leading b-tagged jets are matched to the two lepton candidates which pass the selection criteria above. The distributions are separated according to the number of b-tagged jets in the event. Fair agreement is observed between data and simulation for $m_{\mathrm{t}} = 172.5\,\mathrm{GeV}$ and $\Gamma_{\mathrm{t}} = \Gamma_{\mathrm{t}}^{\mathrm{SM}}$. Overall a slight trend is observed whereby the spectrum in the data is softer than the expected results. Such a trend is compatible with a harder prediction for the top quark p_{T} in POWHEG +PYTHIA 8 [21–23] and a systematic uncertainty due to the mismodelling of the top quark p_{T} will be assigned (see Sec. 4). Moderately boosted events are expected to have a higher fraction of correctly assigned lepton-jet pairs, i.e. where the two legs are from the same

top quark decay. In our analysis, non-boosted pairs are defined with $p_T(\ell, b) \leq 100\,\text{GeV}$, while boosted pairs have $p_T(\ell, b) > 100\,\text{GeV}$. In both =1b and $\geq$2b event categories, the probability of correctly pairing the lepton with the b-jet when they are boosted is expected to be $\approx$63%, versus $\approx$40% in the non-boosted categories.

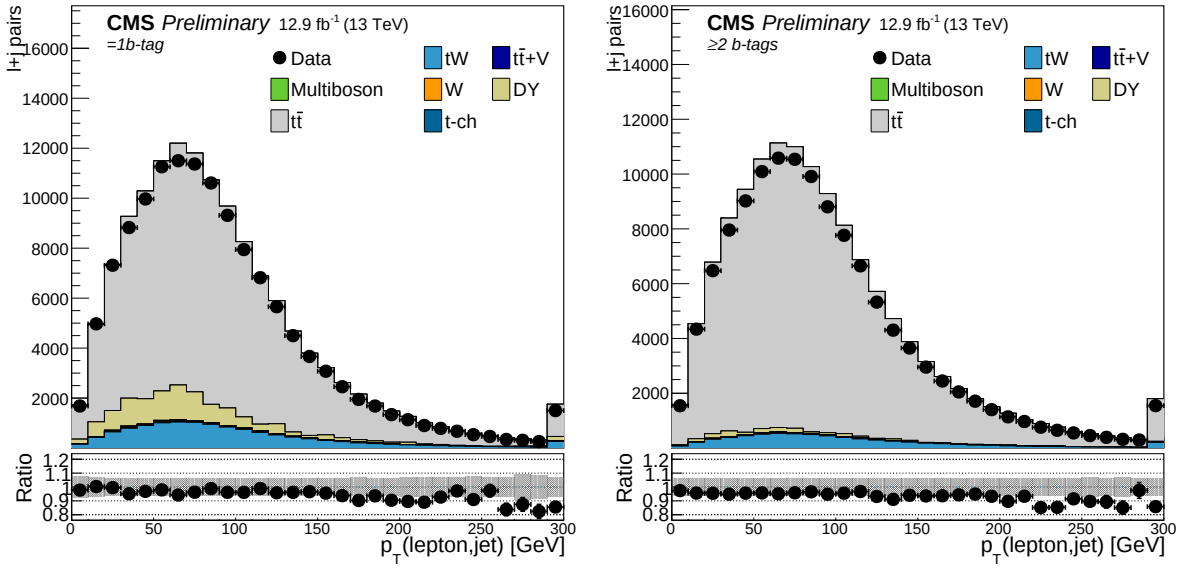

Figure 1: Distributions of the inclusive lepton-b-jet transverse momentum, $p_T(\ell, b)$, for events with $= 1$ (left) or $\geq$2 (right) b-tagged jets. All dilepton channels are combined. The top panels compare the distribution in the data to the simulated expectations, while the bottom panels display the ratio of the two. The shaded band in the bottom panel represents the uncertainty in the prediction due to the limited statistics in the simulation and due to the integrated luminosity.

3 Observable chosen, and its sensitivity to Γ_t

We analyse the inclusive spectrum of the invariant mass of the lepton-b-tagged jet systems ($M_{\ell b}$). The distributions are obtained by pairing the two leading-p_T charged leptons with up to two leading-p_T b-tagged jets and separating according to the number of b-tagged jets and the p_T of the (ℓ, b) system. The masses of all possible lepton-b pairings are stored for a given event. Other selection strategies for the (ℓ, b) pairs considered in the analysis have been tested (minimum mass, minimizing $\Delta R(\ell, b)$, or imposing a cut in this variable), but the optimal sensitivity is expected from the inclusive strategy we have outlined. An alternative analysis using the M_{T2} variable (similar to the one used in [24]) has also been attempted, but leads to slightly wider bounds on Γ_t.

The $M_{\ell b}$ distribution is characterized by an end-point related to the the masses of the t quark and the W boson. At LO, and neglecting the b quark mass, the endpoint is defined as $M_{\ell b}^{\text{max}} = \sqrt{m_t^2 - m_W^2}$, for pairs coming from the same top quark decay. Incorrectly assigned pairs or background pairs are not bound kinematically and often have masses significantly higher than $M_{\ell b}^{\text{max}}$. Nevertheless, at higher orders, and taking into account width effects, there is some spillage of correctly assigned pairs above $M_{\ell b}^{\text{max}}$ [25–32]. While this information may in principle be used to improve the accuracy in the determination of m_t and Γ_t, in this preliminary analysis we perform a measurement calibrated to NLO in the production and LO in the decay simulation of double ($t\bar{t}$) and single (tW) resonant top quarks, where the mass line shape of the top quark follows a relativistic Breit-Wigner distribution.

Figure 2 shows the distributions of the inclusive $M_{\ell b}$ observable in all channels. Fair agreement is observed with expectations obtained for $t\bar{t}$ and tW simulations using $m_t = 172.5\,\text{GeV}$ and $\Gamma_t = 1.324\,\text{GeV}$.

The expected sensitivity of the selected observable to variations in the width is compared to the variations induced by the mass of the top quark in Fig. 3 for the different categories used in the analysis. While most of the sensitivity to the mass is expected near the endpoint (similar to the conclusion found in [24]), variations of the width are expected to impact lower values of the $M_{\ell b}$ observable. Given the absence of higher corrections to the decay of the top quark it is reasonable that no sensitivity to the width is expected above the kinematic endpoint. As such we expect the bounds on the width reported in this analysis to be dominated from the information measured in events with low $M_{\ell b}$ While they display some sensitivity to variations in the top quark width, the non-boosted categories are expected to contribute mostly as control regions for the analysis. The sensitivity of the analysis is expected to be driven by the boosted categories.

4 Systematic uncertainties

Systematic uncertainties for this analysis are treated as nuisance parameters in likelihood fits, described in detail in the next section. The nuisances may reflect a change in the shape of the distribution, the rate of a process, or both. In the fit procedure described in Section 5, we have chosen log-normal distributions to describe these nuisance parameters.

Experimental uncertainties affecting the measurement of $M_{\ell b}$ include:

Pileup: to estimate the impact of the mismodelling of pileup in the simulation, we vary the effective minimum bias cross section by 5% with respect to its initial estimate.

Trigger and selection efficiency: To correct for the performance differences between lepton tracking efficiency, identification and isolation in data and that in simulation, we apply a p_T,η-dependent scale factor, measured with the tag-and-probe method [33–35]. Trigger efficiencies, with respect to the offline selection, are measured using a control sample triggered by uncorrelated E_T^{miss} triggers. The procedure adopted is similar to the one described in [36] and allows for a parametrization of the efficiency and the corresponding uncertainty as functions of the lepton kinematics. Both the uncertainty on the trigger efficiency and on the lepton identification and isolation efficiency scale factors are propagated by re-weighting the simulation after shifting the nominal values by their corresponding uncertainties.

Lepton energy scale: A variation of the lepton energy scale according to its uncertainties is performed independently for muons and electrons.

Jet energy scale and resolution (JES/JER): A p_T- and η-dependent parameterization of the jet energy scale and resolution is used to vary the calibration of the jets in the simulation. The procedure is similar to the one described in [37].

b**-tagging efficiencies:** The nominal efficiency expected in the simulation is corrected by the p_T-dependent scale factors described in [20]. Depending on the flavour of each jet, the b-tagging decision is updated according to the scale factor measured. The scale factor is also varied according to its uncertainty. In the fit we separate the efficiencies for tagging b, c and other jets (light quarks, gluons, or unmatched).

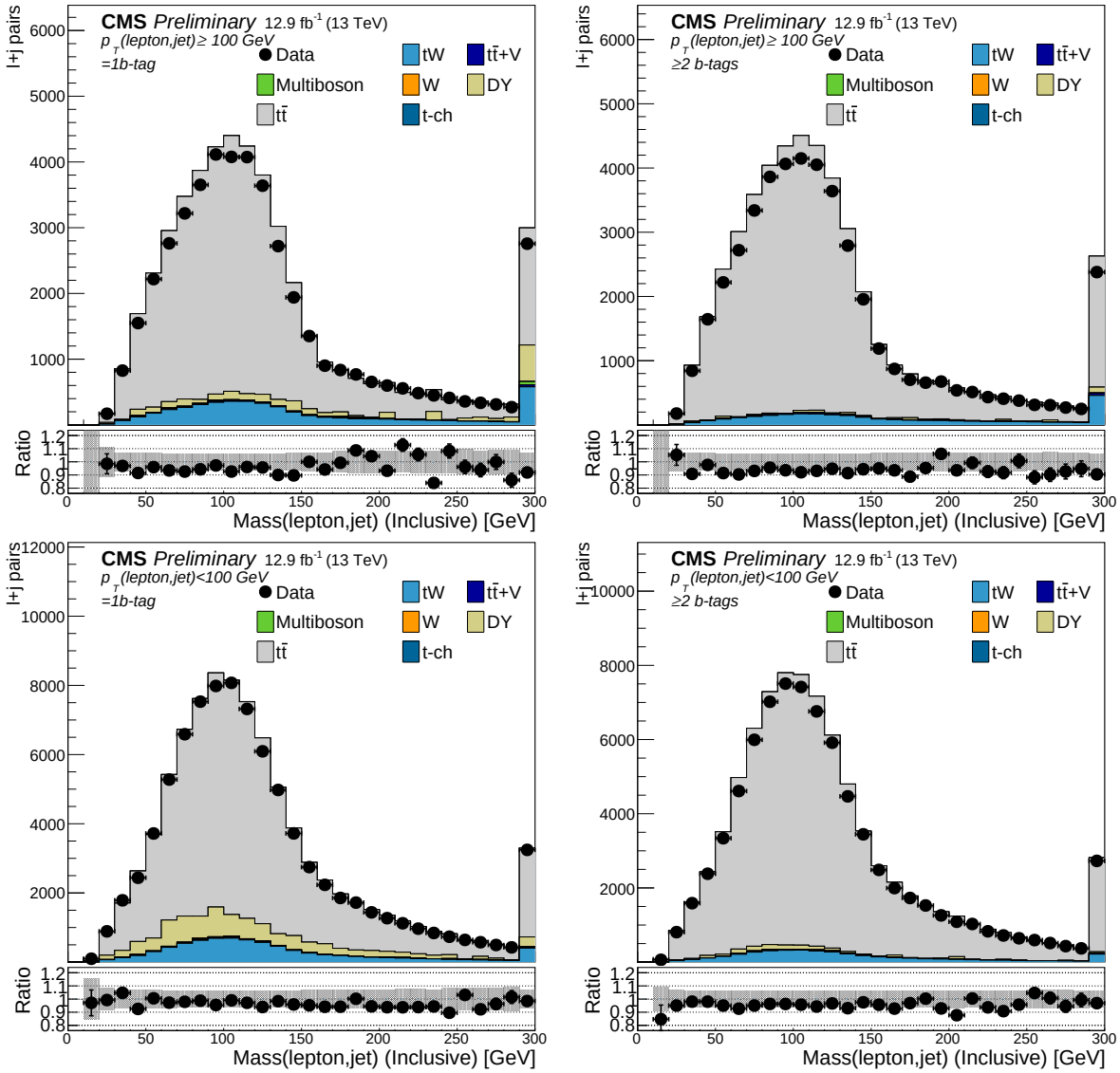

Figure 2: Distribution of the $M_{\ell b}$ observable calculated using up to two leptons and two b-tagged jets per event, for all dilepton channels combined. The plots on the top (bottom) refer to the boosted (non-boosted) category, and the plots on the left (right) correspond to the =1b ($\geq$ 2b) event category. In each plot the top panels compare the distribution in the data to the simulated expectations, while the bottom panels display the ratio of the two. The last bin includes the overflow of the distributions. The shaded band in the bottom panel represents the uncertainty in the prediction due to the limited statistics in the simulation and due to the integrated luminosity.

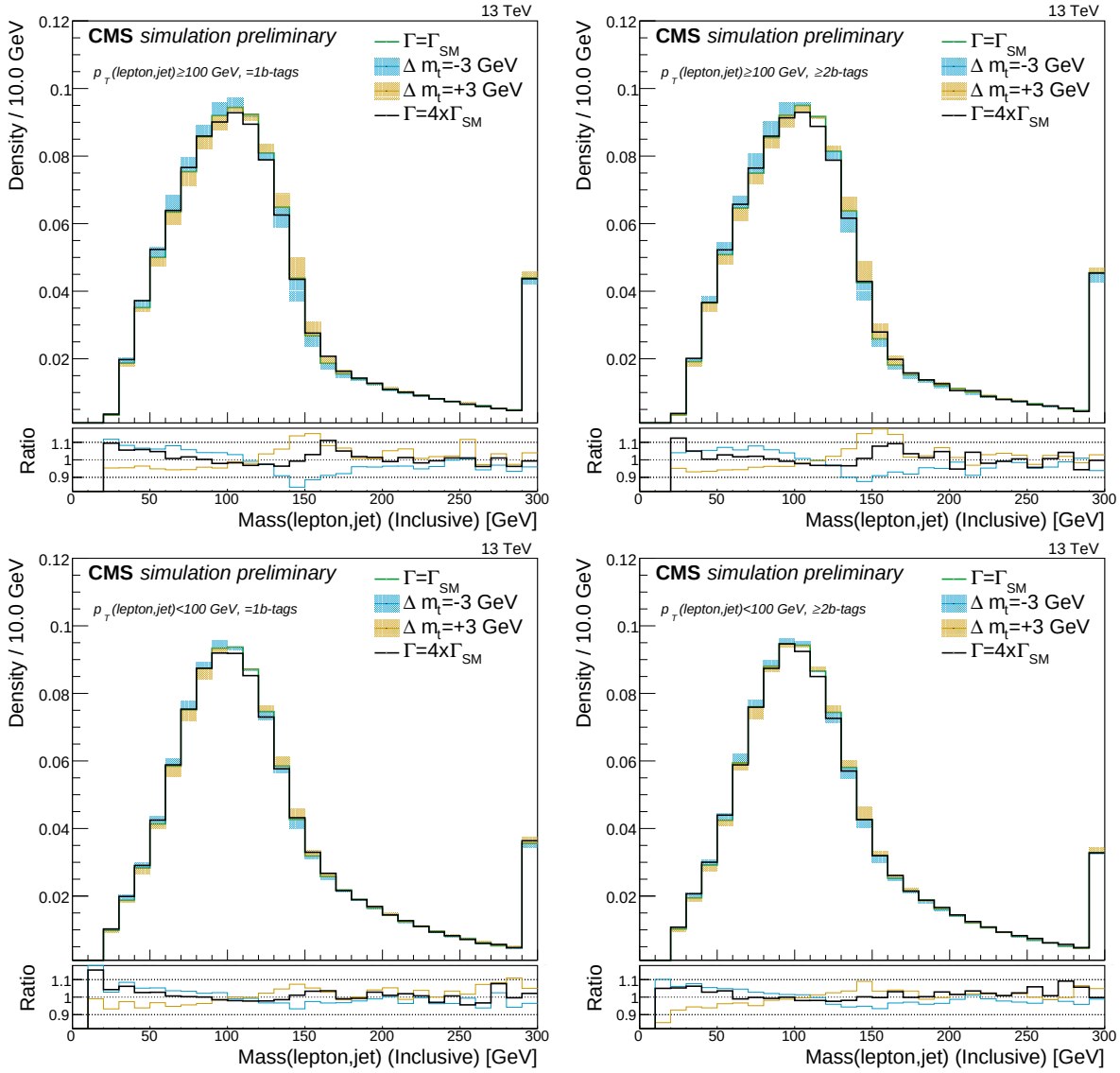

Figure 3: Distribution of the $M_{\ell b}$ variable for simulated POWHEG +PYTHIA 8 events where the top quark mass is varied by ± 3 GeV with respect to 172.5 GeV and the width is varied by a factor of 4 with respect to the SM value. The upper (lower) row of plots describes boosted (unboosted) events, while the left (right) column displays information in the 1b($\geq$ 2b) category. The top panels show the distributions with the last bin displaying the overflow of the histograms while the bottom plot show the ratio with respect to the $m_t = 172.5$ GeV and $\Gamma_t = \Gamma_{SM}$ scenario.

Integrated luminosity: The uncertainty on the integrated luminosity is estimated at 6.2% [6].

Drell-Yan normalisation: The simulated Drell-Yan background events were rescaled by the expected yield calculated from the Z pole mass region, as described in Sec. 2. A systematic uncertainty of 30% is assigned to the normalization of this process uncorrelated accross the different channels.

Other backgrounds: The theoretical uncertainty on the expected cross section for residual backgrounds is included as an uncertainty in the fits.

Theoretical uncertainties may also affect the rate and shape of the $M_{\ell,\mathrm{b}}$ observable. These include:

Choice of the QCD scale: We consider anti-correlated variations of the factorization and renormalization scales (μ_R/μ_F) in the $\mathrm{t\bar{t}}$ sample, by factors of 0.5 and 2. For tW we include a simultaneous variation of μ_R/μ_F by 0.5 and 2 as an uncertainty in the fit.

Matrix Element generator and jet-parton matching scheme: The default simulation is based on POWHEG. We compare with MG5_AMC@NLO+PYTHIA 8 with FxFx matching and assign an uncertainty to the differences in simulation. In the fit we parameterize the effect of the nuisance by mirroring the binwise discrepancies with respect to the nominal information.

Hadronizer choice: The choice of the hadronizer is assigned an uncertainty by comparing the shape and variation of the acceptance between POWHEG hadronized with PYTHIA 8 or HERWIG++. The variation is symmetrized at each bin. The b-tagging efficiency in the HERWIG++ simulation is corrected to match the expected efficiency for the PYTHIA 8 simulation for which the data/MC scale factors are derived [20].

Parton shower scale: Alternative POWHEG +PYTHIA 8 samples in which the parton shower scale choice is varied by a factor of 0.5 and 2 are used in the analysis. This affects the fragmentation and hadronization of the jets initiated by the matrix element calculation as well as the emission of extra jets by the hadronizer.

Top p_{T}: The uncertainty due to the modelling of the top quark p_{T} distribution in the simulation is evaluated by re-weighting it at generator level to match the one measured in data. Scale factors similar to the ones obtained at 8 TeV [38] are used to produce bin-by-bin shape differences for the observable distributions. As this only produces a one-sided uncertainty, we make it two-sided by mirroring the relative differences with respect to the nominal template.

Top mass: The most recent measurement of the top quark mass by CMS yields a total uncertainty of ± 0.49 GeV [1]. In the fits we consider variations of the top mass due to this uncertainty as a nuisance parameter, in a 6σ band at $m_t = 172.5 \pm 3.0$ GeV. Template distributions are generated from Monte Carlo simulated datasets where the generator-level top mass is fixed at either edge of the band.

Parton distribution functions: The parton distribution function (PDF) used to model proton-proton collisions is assigned an uncertainty. The root mean square of 100 replicas of the NNPDF3.0 set is computed and added in quadrature to 2 extra variations corresponding to different choices of α_{S}.

tW/$t\bar{t}$ interference: At NLO QCD, tW production is expected to interfere with $t\bar{t}$ production [39–41]. Two schemes for defining the tW signal in a way which distinguishes it from $t\bar{t}$ production have been compared in our analysis: "diagram removal" (DR) [39], in which all doubly resonant NLO tW diagrams are removed, and "diagram subtraction" (DS) [39, 42], where a gauge-invariant subtractive term modifies the NLO tW cross section to locally cancel the contribution from $t\bar{t}$. The difference between the samples simulated using the two approaches is taken as a systematic uncertainty.

5 Statistical analysis

To test different hypotheses for the top quark width, we analyse likelihood ratios calculated from pairs of shape hypotheses. The adopted procedure is similar to the one used in [43]. Hypotheses differed in the generator-level width, where the null hypothesis was fixed at the SM-predicted $\Gamma_t = 1.324\,\text{GeV}$. Below we denote the null hypothesis as SM. The hypotheses are generated by re-weighting the generator-level top quark mass distribution with ratios of relativistic Breit-Wigner functions [13] corresponding to the alternative and SM hypotheses being tested. The procedure has been validated for the observable used in this analyis, using a dedicated POWHEG simulation with $\Gamma_t = 4 \cdot \Gamma_t^{SM}$. For each hypothesis, a two-dimensional likelihood scan was performed, varying the signal strength ($\mu \equiv \frac{\sigma_{obs}}{\sigma_{SM}}$) and the sample fraction of alternative width hypothesis (denoted x) as parameters of interest. The signal model generated from these parameters was a scaled linear interpolation between SM and alternate hypotheses:

$$N_{\text{signal}} = \mu\left[(1-x)\cdot N_{\text{SM}} + x \cdot N_{\text{alt}}\right] , \tag{1}$$

where N_{signal} is the total expected number of signal events, and N_{SM} (N_{alt}) is the expectation for the SM (alternate) hypothesis. In Equation 1 the expectations for the signal are furthermore expanded to include the $t\bar{t}$ and tW expectations for each hypothesis under test. The overall signal strength therefore corresponds to the ratio of the observed to the expected $t\bar{t}$ +tW cross section. This parameter is profiled in the fit.

Figure 4 compares the expected values of the likelihood as functions of x, for different alternative top quark width hypotheses. The expected likelihoods are obtained using pseudo-data where $\Gamma_t = \Gamma_{SM}$ or $\Gamma_t = 4 \cdot \Gamma_{SM}$. In each case, these are compared with the values of the fit observed in data. Qualitatively, the data prefers an SM-like scenario, with respect to a wide top quark scenario.

The impact of each uncertainty in the fit, discussed in Sec. 4, is determined by repeating the fit after fixing each nuisance to its best-fit value in data and evaluating the difference in the uncertainty attained in the measurement of x. With this procedure we estimate that the dominant uncertainties in the measurement of x for each pair of width hypotheses being tested is due to $t\bar{t}$ and tW modelling and the luminosity, trigger and selection efficiency-related uncertainties. In general, the post-fit nuisance values and corresponding uncertainties are in good agreement with the pre-fit ones.

In order to quantify the separation of the different hypotheses and derive the limits on an SM-like top quark width, we assume a top quark mass of $m_t = 172.5$ GeV and we perform pseudoexperiments to produce distributions of a test statistic defined from the likelihood ratios between the alternate and SM hypotheses:

$$q \equiv -2 \cdot \ln\left(\frac{\mathcal{L}_{\text{alt}}}{\mathcal{L}_{\text{SM}}}\right) , \tag{2}$$

where $\mathcal{L}_{\text{alt}}$ and $\mathcal{L}_{\text{SM}}$ are the likelihoods for the alternate and SM hypotheses, respectively. These distributions are produced both before and after optimizing x, μ, and all other nuisance parameters through a fit to data. Figure 5 demonstrates distributions of the test statistic from pseudoexperiments. The toy experiments display a Gaussian behavior and the quantiles of the distributions are used to evaluate the separation strength of the hypotheses in each test.

The quantiles of the distributions of the test statistics are represented in Fig. 6. Similar behavior is observed in the pre-fit and post-fit model with the data following closely the SM hypothesis.

Hypothesis separation can be measured via the CL_s criterion, which takes into account the value of the test statistic observed in data, $q_{\text{obs.}}$. $\text{CL}_s^{\text{obs.}}$ is defined as the ratio of the areas under each distribution with $q \leq q_{\text{obs.}}$:

$$\text{CL}_s^{\text{obs.}} = \frac{\text{P}(q_{\text{alt.}} < q_{\text{obs.}})}{\text{P}(q_{\text{SM}} < q_{\text{obs.}})} . \tag{3}$$

An analogous criterion for expected results, $\text{CL}_s^{\text{exp.}}$, can be defined by replacing $q_{\text{obs.}}$ with the median of the SM hypothesis distribution:

$$\text{CL}_s^{\text{exp.}} = \frac{\text{P}(q_{\text{alt.}} < q_{\text{SM}}^{\text{median}})}{0.5} \tag{4}$$

Figure 7 shows the evolution of CL_S as a function of the width of the top quark. The value of Γ_t for an SM-like top quark is constrained by fitting the CL_S as a function of generator-level width using a piece-wise quadratic spline, which takes the separation strength into account for all the different input template widths. An exclusion region at a level of 2σ is calculated as the expected generator-level widths yielding $\text{CL}_\text{S} = 0.05$. The expected bounds at the 95% confidence level are $0.6 \leq \Gamma_\text{t} \leq 2.4$ GeV. The observed bounds at the 95% confidence level are $0.6 \leq \Gamma_\text{t} \leq 2.5$ GeV.

6 Conclusion

We have presented limits on the top quark width using $12.9\,\text{fb}^{-1}$ of proton-proton collision data at $\sqrt{s} = 13$ TeV collected by the CMS experiment. Using $\text{t}\bar{\text{t}}$ and tW decay events with two charged leptons in the final state, we reconstruct the $M_{\ell\text{b}}$ observable inclusively using up to two jets identified as stemming from the fragmentation and hadronization of ab quark. The observable is fit for deviations of the width with respect to the SM prediction. Different event categories are included in the fit to improve the sensitivity of the measurement and partially constraint some of the uncertainties. Binary hypothesis tests are then used to bound an SM-like top quark width to $0.6 \leq \Gamma_\text{t} \leq 2.5\,\text{GeV}$ at the 95% CL, with corresponding expected bounds of $0.6 \leq \Gamma_\text{t} \leq 2.4$ GeV for $m_\text{t} = 172.5\,\text{GeV}$. This constitutes the first such direct measurement at the LHC and the most precise direct bound of the top quark width performed to date.

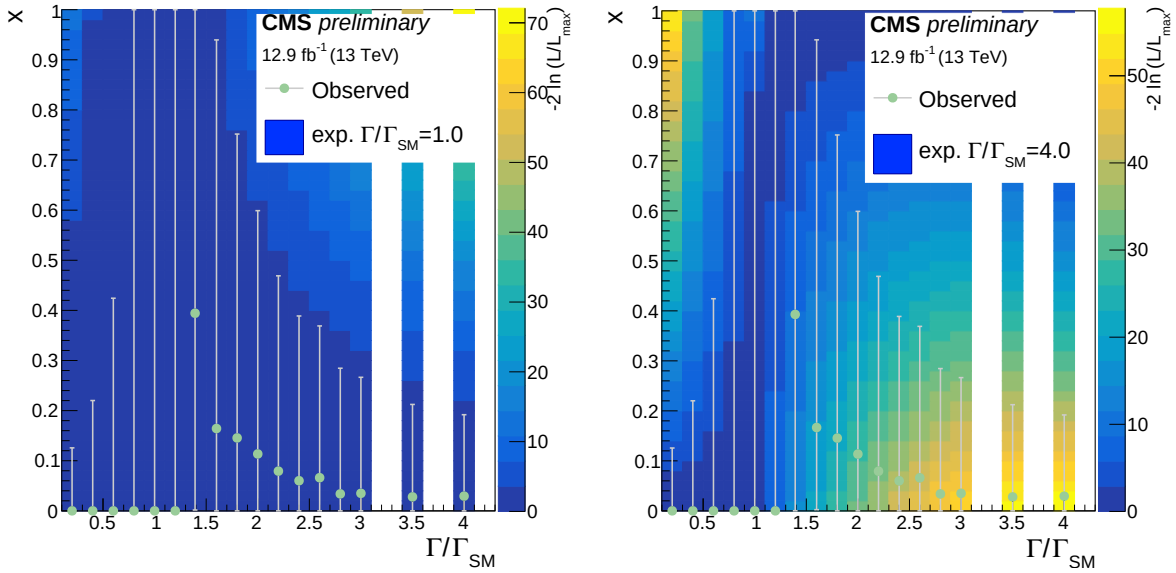

Figure 4: Scan of the likelihood as function of x (the fraction of the alternative width hypothesis) for different top quark width hypothesis. The plot on the left (right) displays the scan expected when $\Gamma_t = \Gamma_{SM}$ ($\Gamma_t = 4 \cdot \Gamma_{SM}$) pseudo-data is used. In both cases the result of the fit to x in the data, after profiling μ, is overlaid for comparison.

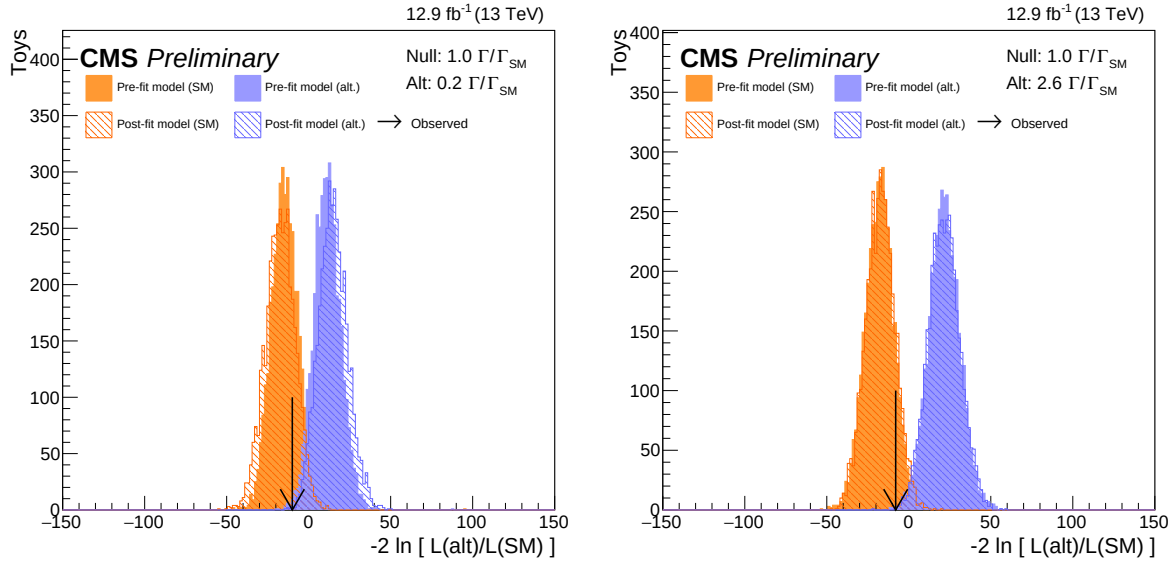

Figure 5: Distributions of the test statistic for pseudoexperiments run on the full with two different alternate hypotheses assuming $\Gamma_t = 0.2 \times \Gamma_{SM}$ (left) and $\Gamma_t = 2.6 \times \Gamma_{SM}$ (right). In both cases the distributions are shown when obtained with the pre-fit model at fixed signal strength and when obtained with the post-fit model after profiling the sinal strength. The values of the test statistics observed in the data are represented by arrows. In both hypotheses, $m_t = 172.5\,\text{GeV}$ is assumed.

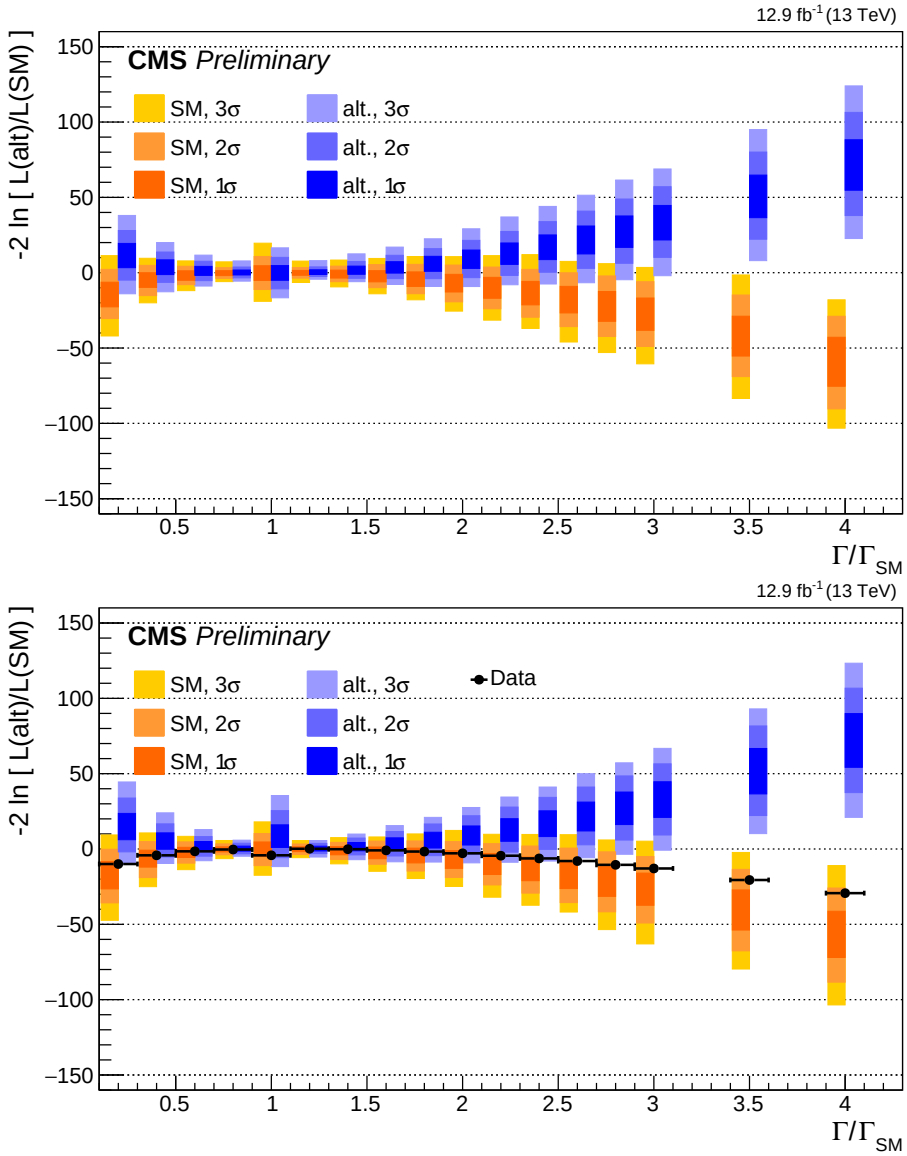

Figure 6: Evolution of the quantiles of the distributions of the test statistics, as a function of the top quark width. The 68%, 95% and 99% CL quantiles are represented by different shades of orange (blue) for the SM (alternative) hypothesis. The plot on the top (bottom) shows the quantiles obtained with the pre-fit (post-fit) model. The values of the test statistics observed in data are represented by the black points in the bottom plot.

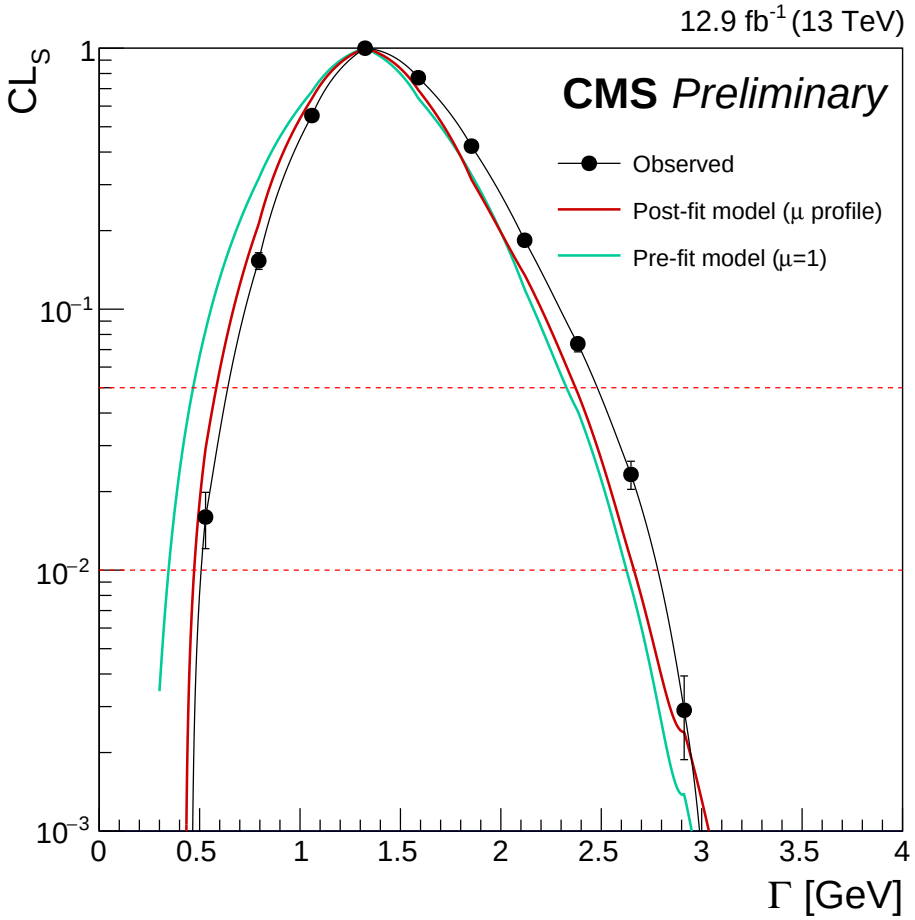

Figure 7: Evolution of the CL_S as a function of the top quark width. The derived limits at the 95% (99%) confidence level are represented as the intersection of the fits to the line at $CL_S = 0.05$ (0.01). The expectations from both the pre-fit and post-fit models are represented by means of a best-fit spline curve.

References

[1] CMS Collaboration, "Measurement of the top quark mass using proton-proton data at $\sqrt{s} = 7$ and 8 TeV", *Phys. Rev. D* **93** (Apr, 2016) 072004, doi:10.1103/PhysRevD.93.072004.

[2] C. P. Yuan, "A new method to detect a heavy top quark at the Tevatron", *Phys. Rev. D* **41** (1990) 42, doi:10.1103/PhysRevD.41.42.

[3] D0 Collaboration, "An improved determination of the width of the top quark", *Phys. Rev.* **D85** (2012) 091104, doi:10.1103/PhysRevD.85.091104, arXiv:1201.4156.

[4] CMS Collaboration, "Measurement of the ratio $\mathcal{B}(\mathrm{t} \to \mathrm{Wb})/\mathcal{B}(\mathrm{t} \to \mathrm{Wq})$ in pp collisions at $\sqrt{s} = 8$ TeV", *Phys. Lett.B* **736** (2014) 33, doi:10.1016/j.physletb.2014.06.076, arXiv:1404.2292.

[5] CDF Collaboration, "Direct measurement of the total decay width of the top quark", *Phys. Rev. Lett.* **111** (2013), no. 20, 202001, doi:10.1103/PhysRevLett.111.202001, arXiv:1308.4050.

[6] CMS Collaboration, "CMS luminosity measurement for the 2015 data taking period", CMS Physics Analysis Summary CMS-PAS-LUM-15-001, 2016.

[7] CMS Collaboration, "The CMS experiment at the CERN LHC", *JINST* **3** (2008) S08004, doi:10.1088/1748-0221/3/08/S08004.

[8] M. Czakon and A. Mitov, "Top++: a program for the calculation of the top-pair cross-section at hadron colliders", *Comput. Phys. Commun.* **185** (2014) 2930, doi:10.1016/j.cpc.2014.06.021, arXiv:1112.5675.

[9] N. Kidonakis, "Top quark production", in *Proceedings, Helmholtz International Summer School on Physics of Heavy Quarks and Hadrons (HQ 2013): JINR, Dubna, Russia, July 15-28, 2013*, pp. 139–168. 2014. arXiv:1311.0283. doi:10.3204/DESY-PROC-2013-03/Kidonakis.

[10] S. Frixione, P. Nason, and C. Oleari, "Matching NLO QCD computations with parton shower simulations: the POWHEG method", *JHEP* **11** (2007) 070, doi:10.1088/1126-6708/2007/11/070, arXiv:0709.2092.

[11] S. Alioli, P. Nason, C. Oleari, and E. Re, "A general framework for implementing NLO calculations in shower Monte Carlo programs: the POWHEG BOX", *JHEP* **06** (2010) 043, doi:10.1007/JHEP06(2010)043, arXiv:1002.2581.

[12] E. Re, "Single-top Wt-channel production matched with parton showers using the POWHEG method", *Eur. Phys. J. C* **71** (2011) 1547, doi:10.1140/epjc/s10052-011-1547-z, arXiv:1009.2450.

[13] T. Sjöstrand, S. Mrenna, and P. Skands, "PYTHIA 6.4 physics and manual", *JHEP* **05** (2006) 026, doi:10.1088/1126-6708/2006/05/026, arXiv:hep-ph/0603175.

[14] T. Sjöstrand et al., "An introduction to PYTHIA 8.2", *Comput. Phys. Commun.* **191** (2015) 159, doi:10.1016/j.cpc.2015.01.024, arXiv:1410.3012.

[15] F. Demartin et al., "The impact of PDF and alphas uncertainties on Higgs Production in gluon fusion at hadron colliders", *Phys. Rev. D* **82** (2010) doi:10.1103/PhysRevD.82.014002, arXiv:1004.0962.

[16] CMS Collaboration, "Underlying event tunes and double parton scattering", CMS Physics Analysis Summary CMS-PAS-GEN-14-001, 2016.

[17] P. Skands, S. Carrazza, and J. Rojo, "Tuning PYTHIA 8.1: the Monash 2013 Tune", *Eur. Phys. J. C* **74** (2014), no. 8, doi:10.1140/epjc/s10052-014-3024-y, arXiv:1404.5630.

[18] CMS Collaboration, "Measurement of the top quark pair production cross section in proton-proton collisions at $\sqrt{s} = 13\,\text{TeV}$", *Phys. Rev. Lett.* **116** (2016) doi:10.1103/PhysRevLett.116.052002, arXiv:1510.05302.

[19] J. Allison et al., "Geant4 developments and applications", *IEEE Trans. Nucl. Sci.* **53** (2006) 270, doi:10.1109/TNS.2006.869826.

[20] CMS Collaboration, "Identification of b quark jets at the CMS Experiment in the LHC Run 2", CMS Physics Analysis Summary CMS-PAS-BTV-15-001, 2016.

[21] CMS Collaboration, "Measurement of particle level differential ttbar cross sections in the dilepton channel at $\sqrt{s}$ = 13 TeV", CMS Physics Analysis Summary CMS-PAS-TOP-16-007, 2016.

[22] CMS Collaboration, "Measurement of the inclusive and differential $\mathrm{t\bar{t}}$ production cross sections in lepton + jets final states at 13 TeV", CMS Physics Analysis Summary CMS-PAS-TOP-16-008, 2016.

[23] CMS Collaboration, "Measurement of the differential cross section for $\mathrm{t\bar{t}}$ production in the dilepton final state at $\sqrt{s} = 13$ TeV", CMS Physics Analysis Summary CMS-PAS-TOP-16-011, 2016.

[24] CMS Collaboration, "Measurement of the top-quark mass in the $\mathrm{t\bar{t}}$ dileptonic channel using the $M_{\mathrm{b},\ell}$, M_{T2}, and $M_{\mathrm{b}\ell\nu}$ observables", CMS Physics Analysis Summary CMS-PAS-TOP-15-008, 2015.

[25] A. Denner, S. Dittmaier, S. Kallweit, and S. Pozzorini, "NLO QCD corrections to WWbb production at hadron colliders", *Phys. Rev. Lett.* **106** (2011) 052001, doi:10.1103/PhysRevLett.106.052001, arXiv:1012.3975.

[26] G. Bevilacqua et al., "Complete off-shell effects in top quark pair hadroproduction with leptonic decay at next-to-leading order", *JHEP* **02** (2011) 083, doi:10.1007/JHEP02(2011)083, arXiv:1012.4230.

[27] A. Denner, S. Dittmaier, S. Kallweit, and S. Pozzorini, "NLO QCD corrections to off-shell top-antitop production with leptonic decays at hadron colliders", *JHEP* **10** (2012) 110, doi:10.1007/JHEP10(2012)110, arXiv:1207.5018.

[28] F. Cascioli, S. Kallweit, P. Maierhfer, and S. Pozzorini, "A unified NLO description of top-pair and associated Wt production", *Eur. Phys. J. C* **74** (2014), no. 3, 2783, doi:10.1140/epjc/s10052-014-2783-9, arXiv:1312.0546.

[29] R. Frederix, "Top Quark Induced Backgrounds to Higgs Production in the $\mathrm{WW}^{(*)} \to \ell\ell\nu\nu$ Decay Channel at Next-to-Leading-Order in QCD", *Phys. Rev. Lett.* **112** (2014), no. 8, 082002, doi:10.1103/PhysRevLett.112.082002, arXiv:1311.4893.

[30] G. Heinrich et al., "NLO QCD corrections to $W^+W^-b\bar{b}$ production with leptonic decays in the light of top quark mass and asymmetry measurements", *JHEP* **06** (2014) 158, doi:10.1007/JHEP06(2014)158, arXiv:1312.6659.

[31] M. V. Garzelli, A. Kardos, and Z. Trcsanyi, "Hadroproduction of $W^+W^-b\bar{b}$ at NLO accuracy matched with shower Monte Carlo programs", *JHEP* **08** (2014) 069, doi:10.1007/JHEP08(2014)069, arXiv:1405.5859.

[32] J. M. Campbell, R. K. Ellis, P. Nason, and E. Re, "Top-pair production and decay at NLO matched with parton showers", *JHEP* **04** (2015) 114, doi:10.1007/JHEP04(2015)114, arXiv:1412.1828.

[33] CMS Collaboration, "Performance of electron reconstruction and selection with the CMS detector in proton-proton collisions at $\sqrt{s} = 8$ TeV", *Journal of Instrumentation* **10** (2015), no. 06, P06005.

[34] CMS Collaboration, "Performance of muon identification in pp collisions at $\sqrt{s} = 7$ TeV", CMS Physics Analysis Summary CMS-PAS-MUO-10-002, 2010.

[35] CMS Collaboration, "Performance of CMS muon reconstruction in pp collisions at $\sqrt{s} = 7$ TeV", CMS Physics Analysis Summary CMS-PAS-MUO-10-004, 2010.

[36] CMS Collaboration, "Measurement of the $t\bar{t}$ production cross section in the eμ channel in proton-proton collisions at $\sqrt{s} = 7$ and 8 TeV", *JHEP* **08** (2016) 029, doi:10.1007/JHEP08(2016)029, arXiv:1603.02303.

[37] CMS Collaboration, "Jet energy scale and resolution in the CMS experiment in pp collisions at 8 TeV", *Submitted to: JINST* (2016) arXiv:1607.03663.

[38] CMS Collaboration, "Measurement of the differential cross section for top quark pair production in pp collisions at $\sqrt{s} = 8$ TeV", *Eur. Phys. J. C* **75** (2015), no. 11, 542, doi:10.1140/epjc/s10052-015-3709-x, arXiv:1505.04480.

[39] S. Frixione et al., "Single-top hadroproduction in association with a W boson", *JHEP* **07** (2008) 029, doi:10.1088/1126-6708/2008/07/029, arXiv:0805.3067.

[40] A. S. Belyaev, E. E. Boos, and L. V. Dudko, "Single top quark at future hadron colliders: complete signal and background study", *Phys. Rev. D* **59** (1999) 075001, doi:10.1103/PhysRevD.59.075001, arXiv:hep-ph/9806332.

[41] C. D. White, S. Frixione, E. Laenen, and F. Maltoni, "Isolating Wt production at the LHC", *JHEP* **11** (2009) 074, doi:10.1088/1126-6708/2009/11/074, arXiv:0908.0631.

[42] T. M. P. Tait, "The tW^- mode of single top production", *Phys. Rev. D* **61** (1999) 034001, doi:10.1103/PhysRevD.61.034001, arXiv:hep-ph/9909352.

[43] CMS Collaboration, "Combination of standard model Higgs boson searches and measurements of the properties of the new boson with a mass near 125 GeV", CMS Physics Analysis Summary CMS-PAS-HIG-13-005, 2013.